Electronic Supplementary Information

The General Synthesis of Ag Nanoparticles Anchored on Silver Vanadium Oxides: Towards High Performance Cathodes for Lithium-ion Batteries

Jiang Zhou,[a] Qiang Liang,[a] Anqiang Pan,[a,] Xuelin Zhang,[a] Qinyu Zhu[a], Shuquan Liang,[a,]* and Guozhong Cao[b,]**

[a] School of Materials Science and Engineering, Central South University, Changsha 410083, P. R. China

[b] Department of Materials Science & Engineering, University of Washington, UW, 98195, USA

Corresponding authors:

pananqiang@gmail.com; lsq@mail.csu.edu.cn; gzcao@u.washington.edu

Experimental section

Chemicals. All chemicals used in our experiments are of analytical purity and used as received without further purification. The Ag/SVOs hybrids were prepared using Ammonium metavanadate (NH_4VO_3, ≥99.0%, Tianjin Guangfu Fine Chemical Research Institute), silver nitrate ($AgNO_3$, ≥99.8%, Sinopharm Chemical Reagent Co., Ltd), and hydrogen peroxide (H_2O_2, ≥30%, Sinopharm Chemical Reagent Co., Ltd) as starting materials.

Synthesis of $Ag/AgVO_3$ hybrid. In a typical procedure, 1 g NH_4VO_3 powder was added into 20 mL of de-ionized water with actively magnetic stirred at room temperature and then 3 ml H_2O_2 solution was added and kept continuously stirred for 20 min to form a bright-yellow solution. A stoichiometric amount (1.4521 g) of $AgNO_3$ was dissolved in 20 ml de-ionized water and then was transferred to the above solution with vigorously stirred at 60 ^oC until it became slurry. Then the slurry was dried overnight in an oven at 60 ^oC. The as-obtained solid mixture was further calcined in air at various temperatures for 4 hours and the final products were obtained. The heating ramp rate was set to 5 $^oC\ min^{-1}$.

Synthesis of $Ag/Ag_2V_4O_{11}$, $Ag/Ag_{0.33}V_2O_5$ and $Ag/Ag_{1.2}V_3O_8$ hybrids. The synthetic procedure was similar to that of $Ag/AgVO_3$ hybrid by only tuning the molar ratios of Ag to V, respectively.

Materials characterization. A combined Differential Scanning Calorimetry (DSC)/Thermogravimetric Analysis (TGA) instrument (Netzsch STA449C, Germany) was used to study the evolution of the precursor in air at a heating rate of 10 $^oC\ min^{-1}$. The phase purity of the as-prepared products were studied by X-ray power diffraction (XRD, Rigaku D/max2500 XRD with Cu Kα radiation, λ=1.54178 Å). To obtain further evidence for the purities and compositions of the as-prepared products, X-Ray photoelectron spectroscopy (XPS) were performed on a K-Alpha 1063 Instrument (Thermo Fisher Scientific, Britain). The SEM images of the as-prepared products were taken with a field emission scanning electron microscopy (SEM, FEI Nova NanoSEM 230). The transmission electron microscopy images and high-resolution transmission electron microscope (HRTEM) images were gathered on transmission electron microscopy (TEM, JEOL JEM-2100F).

Electrochemical measurements. The electrochemical properties were characterized by assembly of coin cells (2025 type coin cell). The cathode slurry was prepared by dispersing the as-prepared products, acetylene black, and polyvinylidene fluoride (PVDF) binder in a weight ratio of

70 : 20 : 10 in a N-methyl-2-pyrrolidone (NMP) solution. The slurry was coated on aluminum foil and dried in a vacuum oven at 90 ^{o}C overnight prior to coin-cell assembly. The coin cells contained cathode electrode, metallic lithium, polypropylene separator, and electrolyte of 1 M solution of $LiPF_6$ in dimethyl carbonate/ethyl methyl carbonate/ethylene carbonate (DMC/EMC/EC) (1 : 1: 1, vol.%), were assembled in a glove box (Mbraun, Germany). The galvanostatic charge/discharge performances of the electrodes were evaluated at room temperature using a Land Battery Tester (Land CT 2001A, Wuhan, China). Cyclic voltammetry (CV) was tested with an electrochemical workstation (CHI604E, China) at a scan rate of 0.05 mV s^{-1}. The electrochemical impedance spectrometry (EIS) was performed on a ZAHNER-IM6ex electrochemical workstation (ZAHNER Co., Germany) in the frequency range of 100 kHz to 10 mHz. The loading of the cathode materials for coin cell test are about 1-2 mg. The specific capacity and current density are based on the weight of active materials only.

Table and Captions

Table S1 Electrochemical properties of SVOs prepared by different methods

Synthesis Method (ref)	Composition	Current Density	Initial Capacity (mA h g^{-1})
Base on $AgVO_3$ nanowires [1]	$AgVO_3$/PANI	30 mA g^{-1}	211
Substrate-assisted hydrothermal [2]	$AgVO_3$	100 mA g^{-1}	≈220
		500 mA g^{-1}	≈163
Hydrothermal [3]	$AgVO_3$	0.01 mA	302
		0.1 mA	273
Hydrothermal [4]	$AgVO_3$	0.1 mA cm^{-2}	104
Sonochemical route [5]	$AgVO_3$	125 mA g^{-1}	102
Rheological phase [6]	$Ag_2V_4O_{11}$	30 mA g^{-1}	272
		120 mA g^{-1}	240
Hydrothermal [7]	$Ag/Ag_2V_4O_{11}$	20 mA g^{-1}	276
		100 mA g^{-1}	150
Hydrothermal [8]	$Ag/AgVO_3$/CNTs	5 mA g^{-1}	268
		1000 mA g^{-1}	197
Solid state reaction [9]	$Ag/AgVO_3$	20 mA g^{-1}	243
		800 mA g^{-1}	198
Hydrothermal [10]	$Ag/AgVO_3$	20mA g^{-1}	285
		1000 mA g^{-1}	188
This work	$Ag/AgVO_3$	5 mA g^{-1}	325
		20 mA g^{-1}	269
		100 mA g^{-1}	259
		500 mA g^{-1}	244
		1000 mA g^{-1}	227
		2000 mA g^{-1}	215
		5000 mA g^{-1}	199

Table S2 Comparison of the electrochemical properties between different SVOs

Composition	Current Density (mA g^{-1})	Initial Capacity (mA h g^{-1})	Capacity (mA h g^{-1}) (cycle number)	Capacity retention
$Ag/AgVO_3$	20	269	None	
	100	259		
	5000	199		
$Ag/Ag_2V_4O_{11}$	20	309	None	
	50	272		
$Ag/Ag_{0.33}V_2O_5$	100	302	220(1) - 194(50)	88.2%
	300	137	137(1) - 132(200)	96.4%
$Ag/Ag_{1.2}V_3O_8$	100	246	246(1) - 164(50)	66.7%

Figures and Captions

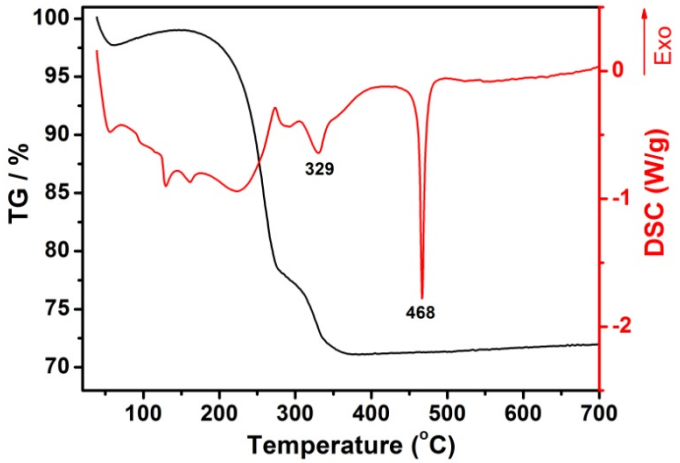

Figure S1. TG and DSC results for the precursor after drying at 60 °C. The temperature ramp rate was set to 10 °C min^{-1}.

Two main weight loss stages are observed on the TG curves. The first one takes a sample weight loss of 2.5 % from ambient temperature to about 63 °C can be attributed to the evaporation of the physically absorbed water of the precursor. The drastic mass loss with 26.5 % on the TG curve and a series of endothermic or exothermal peaks on the DSC curve can be ascribed to the formation of crystalline $Ag/AgVO_3$ hybrid. No obvious endothermic or exothermal peaks in DSC curve after 329 °C and no weight loss in TG curve above 350 °C, indicate the crystallization completed at this temperature range. According to the result, 350 °C, 400 °C and 450 °C were chosen as the calcination temperatures. The sharp endothermic peak on the DSC curve at 468 °C may be caused by the melting of β-$AgVO_3$ crystallites.

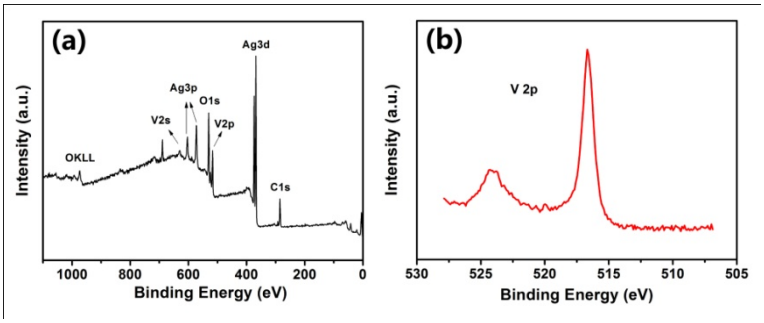

Figure S2. (a) XPS survey spectrum, and (b) V high resolution spectra of $Ag/AgVO_3$ hybrid obtained at 400 ^oC for 4h.

The chemical composition and valence state of the as-obtained $Ag/AgVO_3$ hybrid obtained at 400 ^oC for 4h were further characterized by XPS analysis. The XPS survey spectrum in Figure S2a reveals that the hybrid only consists of carbon, vanadium, silver and oxygen, further confirm its high purity. The binding energies observed in our XPS analysis were calibrated for specimen charging by referencing the C 1s line to 284.8 eV. There are two peaks located at the binding energy of 516.7 and 523.8 eV (Figure S2b), which can be ascribe to a doublet V^{5+} V2p (3/2) and V2p (1/2), respectively.[8]

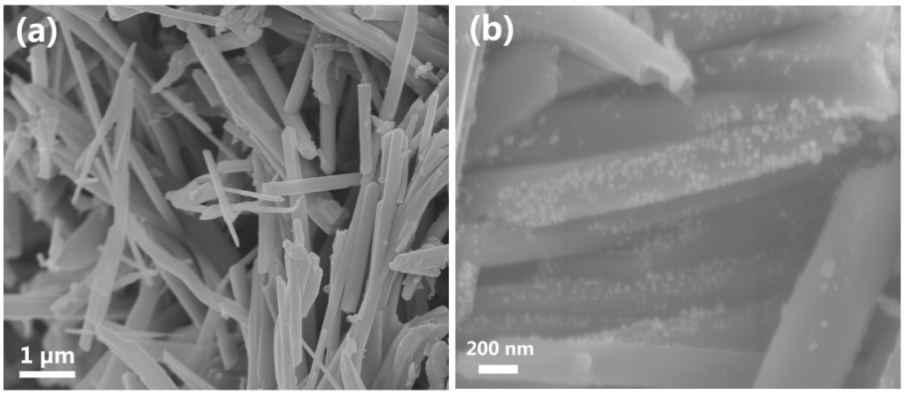

Figure S3. SEM images of $Ag/AgVO_3$ hybrid prepared at 400 ^oC for 4h.

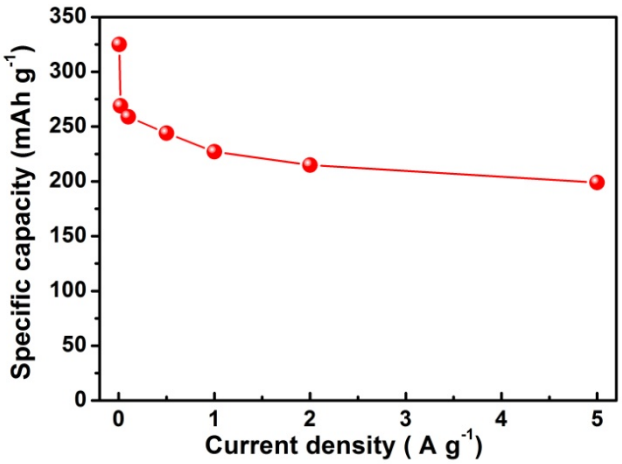

Figure S4. The initial discharge capacities of the $Ag/AgVO_3$ hybrid prepared at 400 °C for 4h at different current densities.

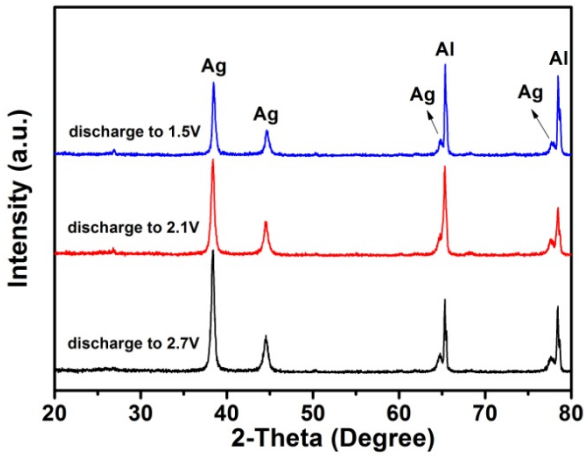

Figure S5. Ex-situ XRD patterns of the $Ag/AgVO_3$ hybrid electrodes discharged to different voltage depths. The applied current density was 20 mA g^{-1}.

The diffraction peaks observed at 2θ=65.133°, 78.227° can be ascribed to centered cubic Al phase (JCPDS Card NO.04-0787), which was used as the current collector. The characteristic diffraction peaks of β-$AgVO_3$ were disappeared, only centered cubic Ag phase can be detected while the electrode discharged to 2.7 V. The diffraction peaks observed at 2θ=38°, 44°, 64° and 77° can be assigned to the (111), (200), (220), (311) planes of Ag phase [JCPDS Card 04-0783]. Similar results are obtained when it is discharged to lower voltages. The results indicate the irreversible phase transformation of Ag and the formation of amorphous phase during discharge process. The formation of silver is also confirmed by Chen's work.[3]

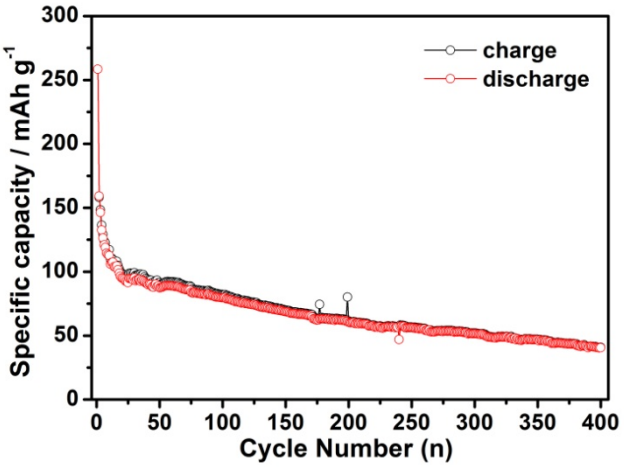

Figure S6. Long-term cycling performance of $Ag/AgVO_3$ hybrid at 100 mA g^{-1}.

Although high initial specific capacity of 259 mA h g^{-1} can be reached for $Ag/AgVO_3$ hybrid, it fastly decreased to 159 mA h g^{-1} at the second cycle at the current density of 100 mA g^{-1}. The capacity fading is become slowly thereafter, and 41 mA h g^{-1} can be retained after 400 cycles, with a fading rate of 0.34 % per cycle of the second cycle.

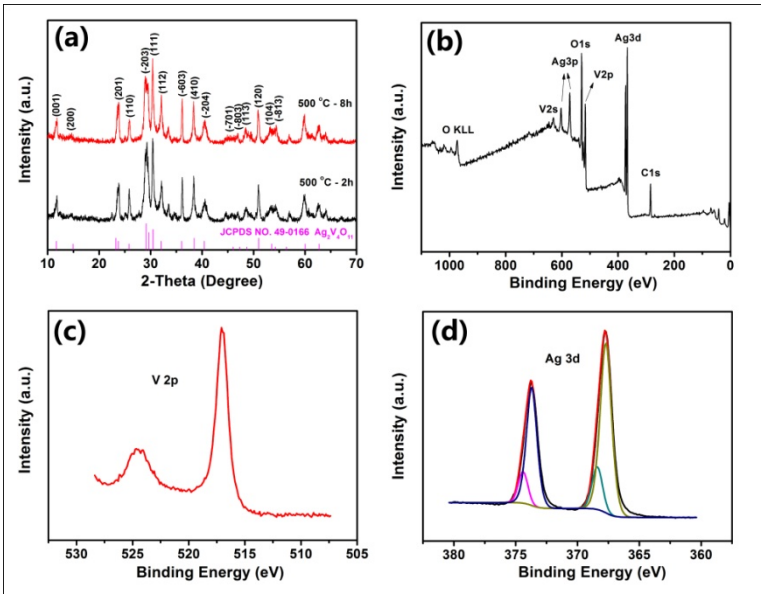

Figure S7. (a) XRD patterns of $Ag/Ag_2V_4O_{11}$ hybrid prepared at different reaction time; (b) XPS survey spectrum, (c) V and (d) Ag high resolution spectra of $Ag/Ag_2V_4O_{11}$ hybrid obtained at 500 ^oC for 2h

As can be seen in Figure S7a, most of the diffraction peaks can be readily indexed to the pure monoclinic $Ag_2V_4O_{11}$ phase [space group: *C2/m*, JCPDS card 49-0166], which is in good agreement with the previous report.[11] The XPS survey spectrum in Figure S7b reveals that the hybrid only consists of carbon, vanadium, silver and oxygen, further confirm its high purity. The binding energies observed in our XPS analysis were calibrated for specimen charging by referencing the C 1s line to 284.8 eV. In Figure S7d, the high-resolution XPS for the Ag 3d region can be divided into two components for the two peaks of Ag 3d (5/2) and Ag 3d (3/2), indicating the presence of different valences of silver species. The two relatively weak peaks located at 368.4 and 374.4 eV can be attributed to Ag^0 Ag3d (5/2) and Ag3d (3/2), respectively. The XPS result gives the evidence of the metallic silver (Ag^0) in the $Ag/Ag_2V_4O_{11}$ hybrid.

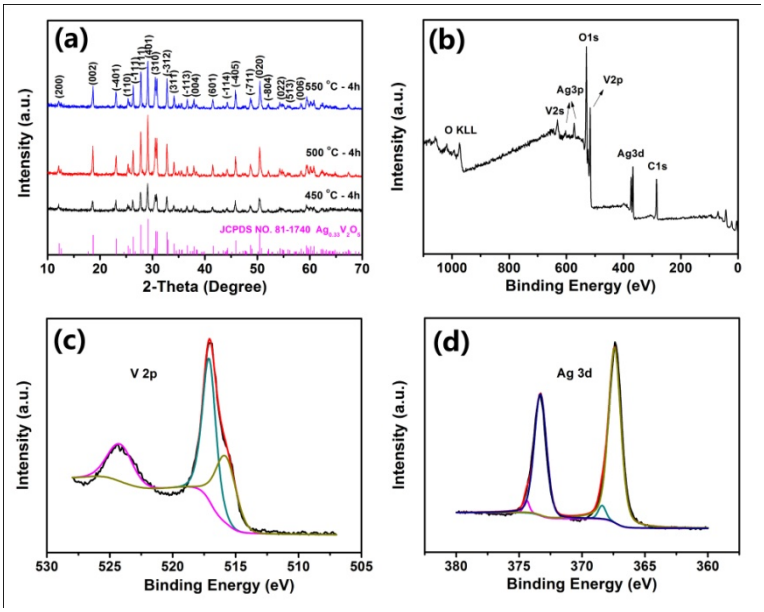

Figure S8. (a) XRD patterns of $Ag/Ag_{0.33}V_2O_5$ hybrids prepared at different temperatures; (b) XPS survey spectrum, (c) V and (d) Ag high resolution spectra of $Ag/Ag_{0.33}V_2O_5$ hybrid obtained at 450 °C for 4h.

As can be seen in Figure S8a, all the diffraction peaks can be readily indexed to the pure monoclinic β-$Ag_{0.33}V_2O_5$ phase [space group: *C2/m* (12), JCPDS card 81-1740], which is in good agreement with the previous reports.[12, 13] The XPS survey spectrum in Figure S8b reveals that the hybrid only consists of carbon, vanadium, silver and oxygen, further confirm its high purity. The binding energies observed in our XPS analysis were calibrated for specimen charging by referencing the C 1s line to 284.8 eV. As seen in Figure S8c, two representative peaks centered at 517.1 and 524.2 eV can be ascribe to a doublet V^{5+} V2p (3/2) and V2p (1/2), respectively, while the other overlapping peak located at 515.8 eV with less intensity indicates the existence of some amount of V^{4+}, confirming the mixture valence state of vanadium atoms in the hybrid, which is consistent with the previous results.[13, 14] In Figure S8d, the two strong peaks at the Ag region of 367.4 and 373.3 eV can be assigned to Ag^+ Ag3d (5/2) and Ag3d (3/2), respectively, while the two relatively weak peaks located at 368.4 and 374.4 eV can be attributed to Ag^0 Ag3d (5/2) and Ag3d (3/2).[3] It is obvious that there are two different silver valence states in the $Ag/Ag_{0.33}V_2O_5$ hybrid, while Ag^+ from $Ag_{0.33}V_2O_5$ and Ag^0 from the metallic silver phase, which confirms the metallic silver in the hybrid.

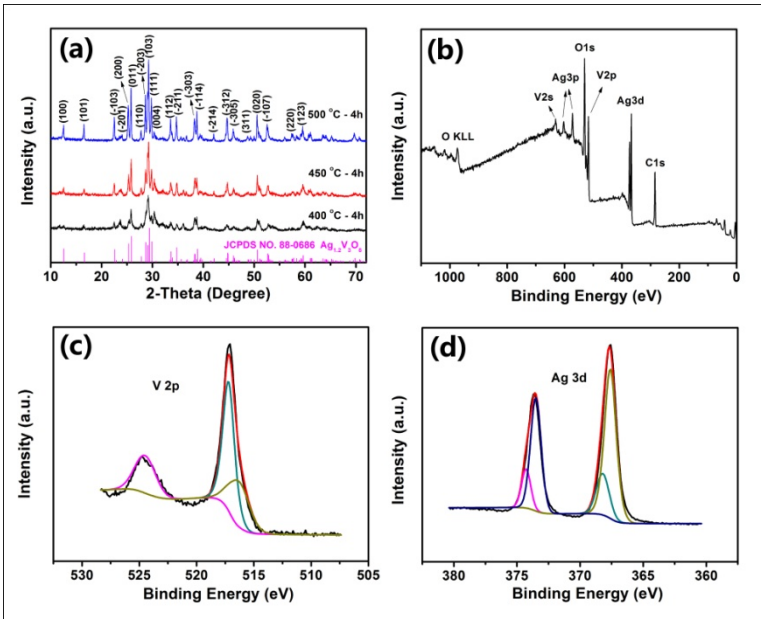

Figure S9. (a) XRD patterns of $Ag/Ag_{1.2}V_3O_8$ hybrids prepared at different temperatures; (b) XPS survey spectrum, (c) V and (d) Ag high resolution spectra of $Ag/Ag_{1.2}V_3O_8$ hybrid obtained at 450 ^oC for 4h.

As can be seen in Figure S9a, all the diffraction peaks can be readily indexed to the pure monoclinic $Ag_{1.2}V_3O_8$ phase with a space group of *$P2_1/m(11)$* [JCPDS card 88-0686], which is in good agreement with the previous reports.[15, 16] There is an asymmetry in the high-resolution XPS for the V 2p region (Figure S9c), which can be due to the presence of different valences of vanadium atoms. The core level at 517.2 eV with the dominant V signal assigned to V^{5+}, while the core level at 515.8 eV with the minor V signal assigned to V^{4+}, which confirms the mixture valence state of vanadium atoms in the hybrid.[15] As can be seen in Figure S9d, the two relatively weak peaks located at 368.2 and 374.27 eV can also be observed, corresponding to the Ag^0 Ag3d (5/2) and Ag3d (3/2), respectively. The XPS result also confirms the metallic silver in the $Ag/Ag_{1.2}V_3O_8$ hybrid.

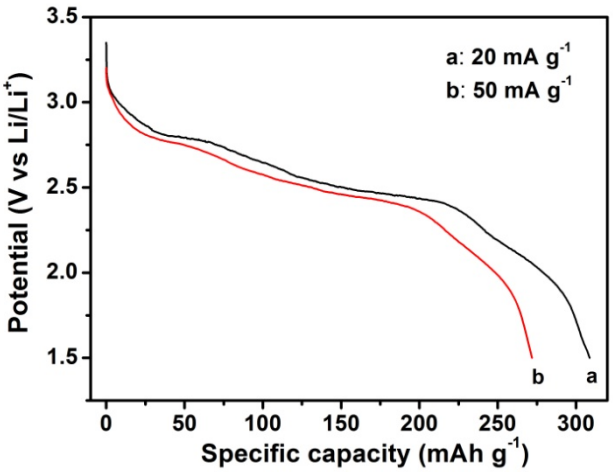

Figure S10. Initial discharge curves at different current densities of $Ag/Ag_2V_4O_{11}$ hybrid prepared at 500 ^oC for 2h.

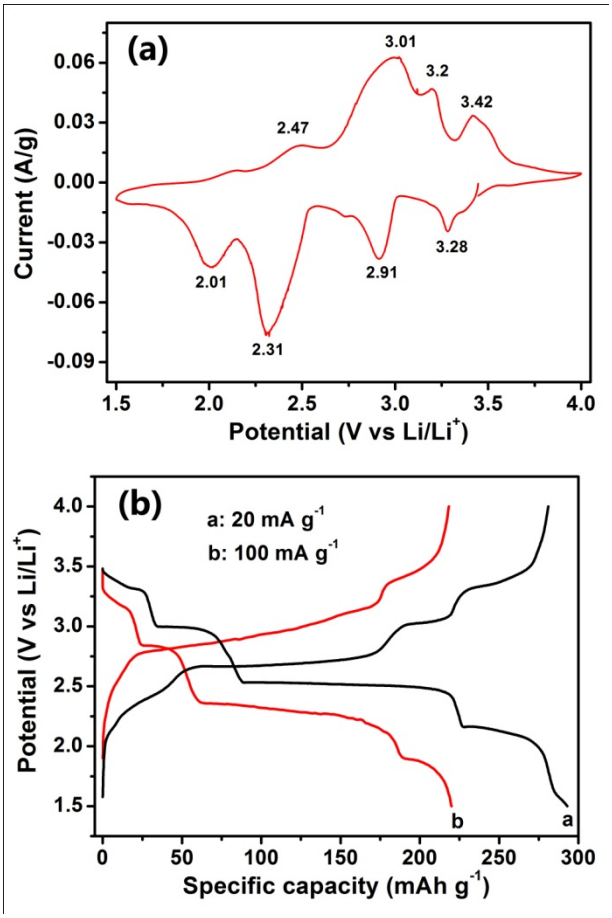

Figure S11. (a) Initial cyclic voltammetry (CV) curve and (b) initial discharge/charge curves at different current densities of $Ag/Ag_{0.33}V_2O_5$ hybrid prepared at 450 ^oC for 4h.

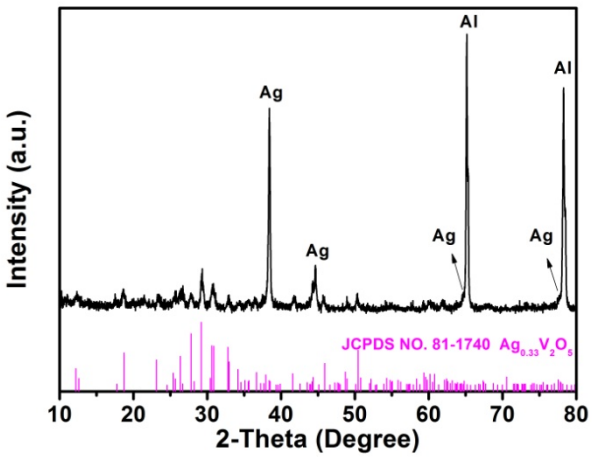

Figure S12. Ex-situ XRD pattern of the $Ag/Ag_{0.33}V_2O_5$ hybrid electrode after 50 cycles. The applied current density was 100 mA g^{-1}.

References

1. L. Mai, X. Xu, C. Han, Y. Luo, L. Xu, Y. A. Wu and Y. Zhao, *Nano Lett.*, 2011, **11**, 4992-4996.
2. C. Han, Y. Pi, Q. An, L. Mai, J. Xie, X. Xu, L. Xu, Y. Zhao, C. Niu, A. M. Khan and X. He, *Nano Lett.*, 2012, **12**, 4668-4673.
3. S. Zhang, W. Li, C. Li and J. Chen, *J. Phys. Chem. B*, 2006, **110**, 24855-24863.
4. C. S. Rout, U. K. Gautam, Y. Bando, D. Rangappa, X. Fang, L. Li and D. Golberg, *Sci. Adv. Mater.*, 2010, **2**, 407-412.
5. C. Mao, X. Wu and J.-J. Zhu, *J. Nanosci. Nanotech.*, 2008, **8**, 3203-3207.
6. X. Cao, H. Zhan, J. Xie and Y. Zhou, *Mater. Lett.*, 2006, **60**, 435-438.
7. Z. Chen, S. Gao, R. Li, M. Wei, K. Wei and H. Zhou, *Electrochim. Acta*, 2008, **53**, 8134-8137.
8. L. Liang, H. Liu and W. Yang, *Nanoscale*, 2013, **5**, 1026-1033.
9. S. Liang, J. Zhou, A. Pan, X. Zhang, Y. Tang, X. Tan, T. Chen and R. Wu, *J. Power Sources*, 2013, **228**, 178-184.
10. S. Liang, J. Zhou, X. Zhang, Y. Tang, G. Fang, T. Chen and X. Tan, *CrystEngComm*, 2013, **15**, 9869-9873.

11. Y. Xu, X. S. Han, L. Zheng, S. Q. Wei and Y. Xie, *Dalton T.*, 2011, **40**, 10751-10757.
12. W. Hu, X. B. Zhang, Y. L. Cheng, C. Y. Wu, F. Cao and L. M. Wang, *ChemSusChem*, 2011, **4**, 1091-1094.
13. Y. Liu, Y. Zhang, M. Zhang and Y. Qian, *J. Cryst. Growth*, 2006, **289**, 197-201.
14. Y. Xu, X. Han, L. Zheng, W. Yan and Y. Xie, *J. Mater. Chem.*, 2011, **21**, 14466-14472.
15. C. Wu, H. Zhu, J. Dai, W. Yan, J. Yang, Y. Tian, S. Wei and Y. Xie, *Adv. Funct. Mater.*, 2010, **20**, 3666-3672.
16. S. Liang, T. Chen, A. Pan, J. Zhou, Y. Tang and R. Wu, *J. Power Sources*, 2013, **233**, 304-308.